The International Journal of Advanced Manufacturing Technology (2019) 102:2183–2193
https://doi.org/10.1007/s00170-018-03225-5

ORIGINAL ARTICLE

Design, numerical simulation, and experimental validation of a novel electromagnetic blank holding system for conventional drawing process

Hao Li[1] · Qiang Wang[1] · Fang He[2] · Yayun Zheng[2] · Yaqian Sun[1]

Received: 6 August 2018 / Accepted: 13 December 2018 / Published online: 23 January 2019

Abstract
In this paper, a novel electromagnetic blank holding system (EBHS) for a conventional drawing process is proposed. The system is created to substitute mechanical or hydraulic blank holder force (BHF) with mutually attractive electromagnetic force (EMF). The winding type of electromagnetic coils is determined as a single-coil through numerical simulation. For avoiding the fluctuation of the magnitude of BHF, direct current is chosen to generate BHF. Corresponding magnetic circuit model of the electromagnetic blank holding device (EBHD) has been established to find the mathematical relationship between EMF and input voltage. Besides, several groups of EMF testing data are measured to prove the correction of deduced expression. To validate the feasibility of the novel system, corresponding numerical simulation and experiment have been carried out. It is worth to mention that the cylindrical parts created by simulation and experiment at different BHF agree well with each other. Additionally, the thickness reduction rate of drawn part is controlled at a reasonable level with the application of EBHS, which well validates the effectiveness of the EBHS.

Keywords Electromagnetic force · Blank holder force · Numerical simulation · Experimental validation

1 Introduction

Blank holding is a critical technology in the field of sheet metal forming. Traditionally, blank holder force (BHF) is mainly provided by rubber, mechanical spring, nitrogen cylinder, and hydraulic system [1, 2], which always performs poorly in flexible control and quick response to BHF. To overcome the difficulty, a novel blank holding technology with the use of electromagnetic force (EMF) has been created to substitute the conventional ones in recent years. The potential advantage of this technology is that the EMF can be flexibly and accurately adjusted in comparison with conventional BHF.

In recent years, the electromagnetic blank holding system (EBHS) is mainly applied in two broad fields: electromagnetic forming and conventional drawing. To electromagnetic forming, the forming time merely required several milliseconds. Therefore, the application time of BHF with this technology is always extremely transient. In addition, alternating current is usually used in electromagnetic forming, which will cause the variable magnitude of BHF during sheet metal drawing process. To the study of the technology, Li et al. [3–6] applied a dual-coil to create a pulsed attractive electromagnetic force and they investigated the acquirement of a large drawing ratio by using an assisted dual-coil to offer radial Lorentz force in an electromagnetic forming process. Furthermore, they studied plastic deformation behavior of sheet metal with augmenting radial Lorentz force during sheet metal drawing and raised a magnetic pulse spot welding (MPSW) process based on the electromagnetic blank holding technology [7]. Because a magnetic system may induce unexpected coil temperature rise, Cao et al. [8] proposed a new discharge circuit configuration with a crowbar circuit to control the discharge current flowing in the tool coil. Different from electromagnetic blank holder designed in [3], Huang et al. [9] proposed a blank holder driven by a capacitor bank and a conductive ring. The created system can generate a pulsed BHF ranging from 0 to 1000 kN at different discharge voltages with an arise time of more than 5 ms. Compared with the investigations on the

✉ Qiang Wang
me_wangq@ujn.edu.cn

[1] School of Mechanical Engineering, University of Jinan, Jinan 250022, China

[2] School of Electrical Engineering, University of Jinan, Jinan 250022, China

technology of electromagnetic forming, conventional drawing relying on electromagnetic blank holding technology is seldom studied in recent years. Based on a conventional drawing of sheet metal, Seo [10] proposed an electromagnetic blank restrainer (EMBR), the intrinsic property of which is making use of magnetic attraction on the ferrous sheet metal. Additionally, Fan et al. [11, 12] created a compound-forming method of cylindrical part drawing by using hydraulic forming and electromagnetic pulse-assisted forming. Mo et al. [13–15] advanced the drawing process of the cylindrical part with the use of incremental electromagnetic-assisted technology. Besides, they applied this technology into the investigation on the forming process and shape control of aluminum alloy [16, 17] and tube forming [18]. Cui et al. [19] created a sheet metal forming approach combined with electromagnetic forming and traditional stamping. With the usage of multidirectional EMF, they extremely reduced the maximum thickness thinning ratio of the cylindrical part.

The theoretical deduction is always the preliminary of novel system design. Wang et al. [20] established a magnetic circuit model to study the relationship between large imbalance evaluation and the dynamic electromagnetic force. Paese et al. [21] proposed a numerical procedure to calculate the EMF in thin circular flat plates by using a spiral coil as an actuator. Okoye et al. [22] established equations about the mechanical characteristics during the electromagnetic forming process. Akbar et al. [23] modeled and proposed the calculation procedure of field intensity on electromagnetic flat sheet forming based on Biot-Savart law.

For exploring the feasibility of a created system, numerical simulation and experimental validation are always critical to be conducted. Guo et al. [24] investigated the forming effect of the panels under different electromagnetic incremental forming process conditions through experiments. Shang et al. [25] developed a new approach to electromagnetically assisted sheet metal stamping. The feasibility of the method had been validated by experiments. Arumugam et al. [26] measured the hardness of the workpiece before and after electromagnetic forming. Besides, a microstructure study was conducted by scanning electron microscope. Long et al. [27] studied electromagnetic superposed forming (EMSF) with analytical and numerical simulation. Li et al. [28] proposed a numerical model of electromagnetically assisted stamping system and it could successfully simulate the combined quasi-static-dynamic process. Furthermore, the numerical results predicted the experimental ones. Similar analysis work had also been carried out by Liu et al. [29].

In this investigation, a novel EBHS for conventional cylindrical part drawing is proposed. The mathematical formula of EMF has been deduced and the feasibility of the novel system has been validated through corresponding numerical simulation and experiments.

2 Principle and design of EBHS

2.1 Principle and configuration design of EBHD

In this study, a novel EBHS for conventional drawing process has been designed. The schematic of the assembly of the electromagnetic blank holding device (EBHD) and sheet metal drawing system has been shown in Fig. 1. In this system, the EMF used for blank holding is generated by the direct current. The whole system can be divided into three sub-systems: (1) drawing system, (2) electromagnetic blank holding system, and (3) fixture system.

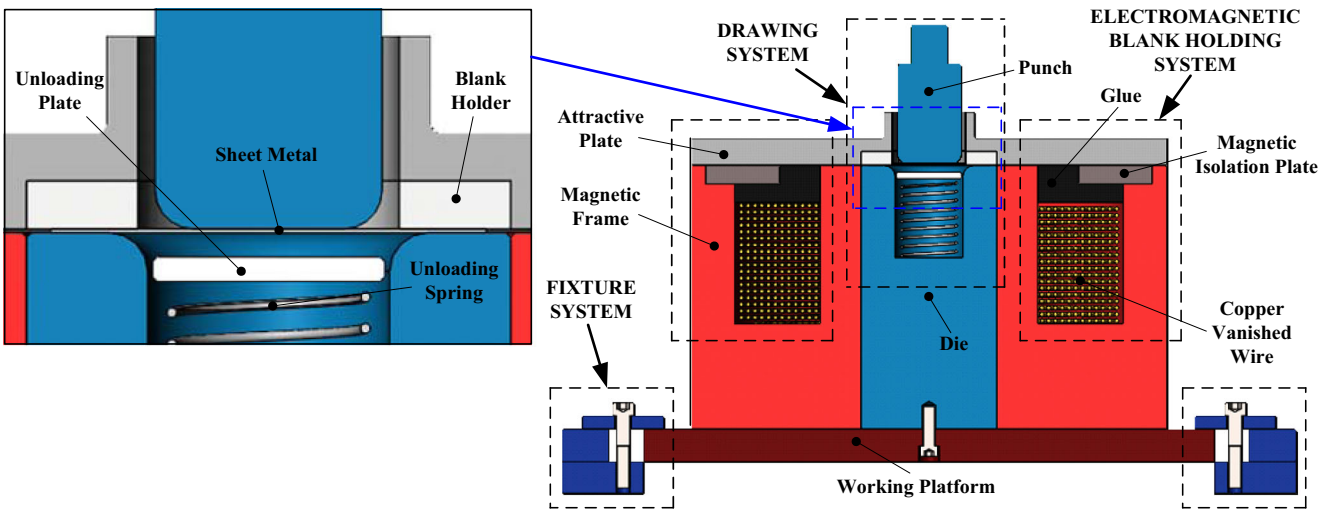

Fig. 1 Schematic of the assembly of EBHD and sheet metal drawing system

Drawing system is applied to the draw sheet metal, which constitutes drawing tools and sheet metal. Besides, a mechanical spring is installed on the bottom of die, which is used to automatically unload workpiece. In the electromagnetic blank holding system, the coils can be winded into a single-coil type or trail-coils type, and concrete coils structure will be discussed in the next section. For avoiding effecting the magnitude of EMF due to unnecessary movement of copper vanished wire, a 6302 glue is poured into the remaining space of magnetic frame. For conveniently alternating drawing tool, a certain amount of clearance is left between the EBHD and the drawing die. In this case, the drawing system is not integrated with the EBHD and the required parts with different shapes will be obtained by changing the shapes of the drawing tool. Additionally, a magnetic isolation plate is designed to decrease the loss of magnetic induction intensity. Fixture system is served as fixing the EBHD on the universal material testing machine. Especially, drawing die and baseboard are tightly fixed on the working platform of the press with the usage of designed fixture system.

The working principle of the designed EBHD is to substitute a conventional BHF into EMF during the drawing process. At first, the amplitude of the direct current is adjusted to the expected magnitude. Nearly at the same time, an attractive electromagnetic BHF will be created in the working gap due to an induced electromagnetic field. When the drawing process begins, the punch starts moving down to draw sheet metal with the EMF applying on the margin of the sheet metal. As the drawing process is over, the demagnetizing process of the EBHD will be conducted and the drawn work piece will be automatically taken out by unloading spring and unloading plate. External profile of the EBHD is shown in Fig. 2.

2.2 Design and simulation testing of coil system

To effectively increase the electrical conductivity of coils, the material chosen for the coil system is copper. For making the EBHD more easily to create a larger BHF applying on the flange region of the cylindrical part, two types of coil structure are discussed. The schematic of the corresponding winding types has been shown in Fig. 3. The first winding type is to make the coils uniformly winded on the inner wall of the magnetic frame. Differently, the other winding type of coils is to wind one coil into several sub-coils and make them uniformly distributed at the bottom of the magnetic frame.

Fig. 2 Eternal profile of the EBHD. (1) Punch. (2) Magnetic plate. (3) Magnetic frame. (4) Baseboard of the device

According to the two types of coils, a group of comparative simulations about the distribution of magnetic flux intensity has been conducted by ANSYS/Multiphysics. Testing parameters have been given in Table 1.

Electromagnetic simulation results have been shown in Fig. 4. From Fig. 4 a and b, it can be easy to see that the maximum magnetic flux intensity occurs in the surrounding of the blank holder when using a single-coil system. Respectively, the larger magnetic flux intensity will occur in the surrounding of sub-coils with the application of the trail-coils system. Besides, it can be also learned that the maximum amplitude of magnetic flux density using a single-coil system is up to 2.27 Wb/m^2, which is 56.68 times larger than that by applying trail-coils system with the utilization of the same number of windings and the amplitude of the direct current. Therefore, it is clear that the conventional single-coil system is more beneficial to enhance BHF created by EBHD. Based on the discussion above, the single-coil winding type is utilized in this study.

3 Theoretical computation of EMF created by EBHD

In this study, magnetic circuit analysis is applied to establish the mathematical relationship between BHF and input voltage. Because of the symmetry of the system frame, the magnetic circuit model of the EBHD can be established as shown in Fig. 5. Besides, corresponding structural parameters have been given in Table 2.

where "H_1," "H_2," and "H_3" are respectively the height of the magnetic frame, the depth of circular groove of the magnetic frame, and the thickness of attractive plate. "r_3," and "r_4" are the radius from the device center to the inner wall of the magnetic frame and the radius of the EBHD.

Making reference to [16], the calculating equation of the total voltage can be described as Eq. (1):

$$U = \sqrt{(IX_L)^2 + (IR)^2} = I\sqrt{\omega^2 N^4 (G_\delta + G_l)^2 + R^2} \qquad (1)$$

where I and X_L are the winding excitation current and the reactance, R and N are the resistance of the winding and the turns of coils, ω is the angular frequency of the exciting current, and G_δ and G_l are the magnetic permeance of the total working air gap and the leakage permeance. Since the current

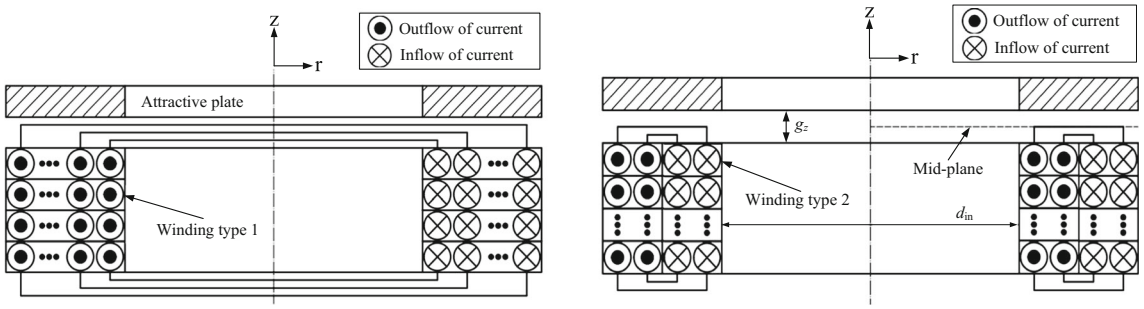

(a) Single-coil type (b) Trial-coils type

Fig. 3 Two critical wrapping types of coils. **a** Single-coil type. **b** Trial-coils type

applied in this novel system is direct current, the value of ω can be regarded as zero. Therefore, Eq. (1) can be simplified as Eq. (2):

$$U = IR \tag{2}$$

Based on the established magnetic circuit model, the expression of excitation current can be acquired by flux division, which is given in Eq. (5). Equation (3) and Eq. (4) show the expression of air gap flux$\Phi_{\delta m}$and the total leakage fluxΦ_{lm}.

$$\frac{\Phi_{\delta m}}{G_\delta} = \frac{\Phi_{lm}}{G_l} \tag{3}$$

$$\Phi_m = \Phi_{\delta m} + \Phi_{lm} = \sigma\Phi_{\delta m}, \quad \sigma = 1 + \frac{G_l}{G_\delta} \tag{4}$$

$$I = \frac{\Phi_m}{(G_\delta + G_l)N} \tag{5}$$

where σ is the leakage flux coefficient and N is the number of windings.

Relying on Maxwell classical magnetic theory, the expression of EMF can be preliminarily written as Eq. (6):

$$F_{\text{mag}} = -\frac{1}{2}U_\delta^2\left(\frac{dG_\delta + dG_l}{d\delta}\right) \tag{6}$$

Table 1 Testing parameters required by magnetic simulation

Process variable	Value	Process variable	Value
Magnitude of DC/A	0.6	Element type of tool	Solid96
Diameter of wire/mm	Φ0.75	Type of coils system	Racetrack coil
Size of air gap/mm	0.3	Size of cross section of winding/mm^2	6900

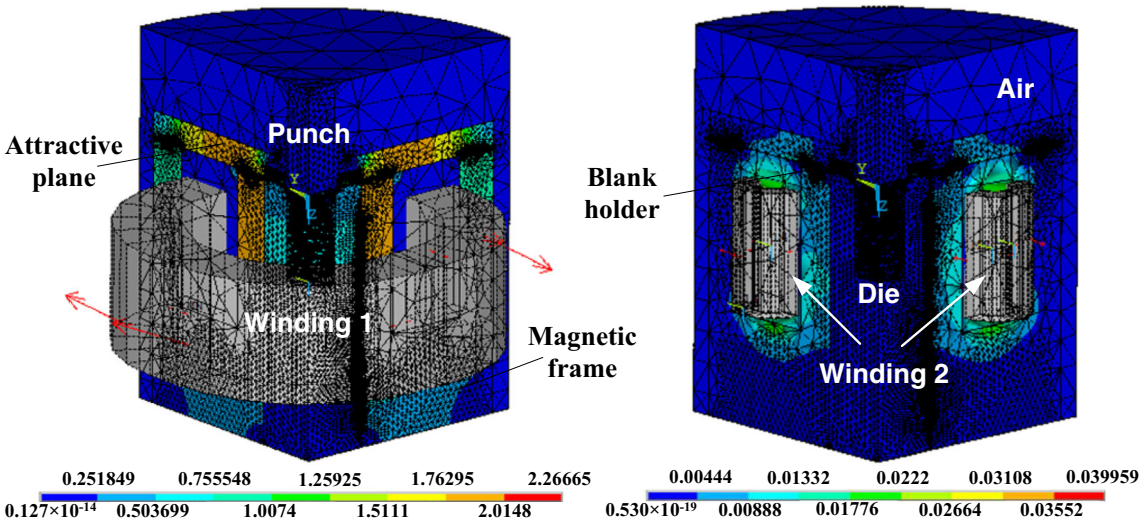

(a) Single-coil system (b) Trail-coils system

Fig. 4 Comparison of the created magnetic flux intensity of the two types of coils structure. **a** Single-coil system. **b** Trail-coils system

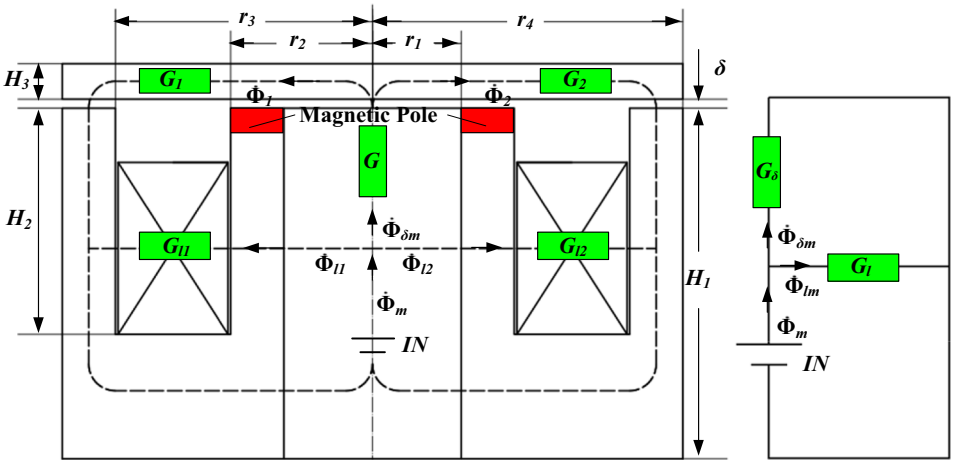

(a) Magnetic circuit model of the EBHD (b) Simplified magnetic circuit model of the EBHD

Fig. 5 Established magnetic model. **a** Magnetic circuit model of the EBHD. **b** Simplified magnetic circuit model of the EBHD

Table 2 Corresponding structural parameters of the EBHD

Parameter/ mm	Value	Parameter/ mm	Value
r_1	50	H_1	199.5
r_2	85	H_2	130
r_3	145	H_3	20
r_4	175	δ	0.3

Table 3 Corresponding parameters of the EBHD

Parameter	Value	Parameter	Value
N	1397	l/mm	596
μ_r/H/m	4000	ρ/Ωm	1.7×10^{-8}
μ_0/H/m	$4\pi \times 10^{-7}$	A_{coil}/m^2	4.42×10^{-7}
S/mm^2	3710	L_{coil}/m	7069

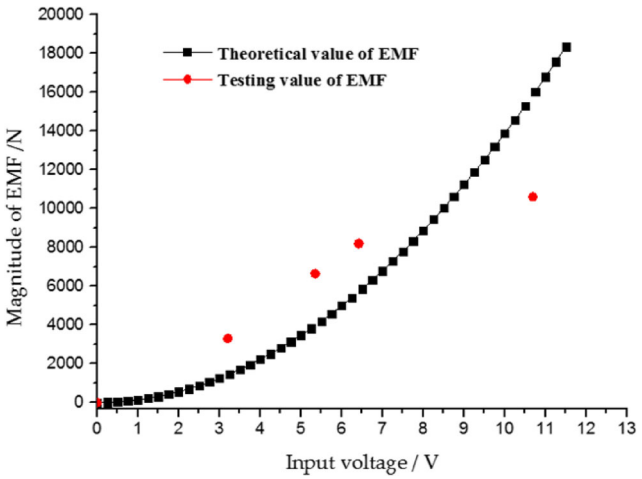

Fig. 6 Theoretical and EMF testing value

where U_δ and δ are the magnetic pressure drop and working air gap, F_{mag} is the EMF.

According to the calculation of U_δ in the Maxwell formula, EMF can be inferred as Eq. (7):

$$F_{mag} = -\frac{1}{2}\left(\frac{\Phi_{\delta m}\delta}{\mu_0 S}\right)^2\left(\frac{-\mu_0 S}{d\delta}\right) = \frac{1}{2}\frac{\Phi_{\delta m}^2}{\mu_0 S} \tag{7}$$

where μ_0 is the permeability of the vacuum and S is the area of the magnetic pole.

Combining with Eqs. (2), (4), (5), and (7), the relationship between the EMF and input voltage has been inferred as Eq. (8):

$$F_{mag} = \frac{U^2 G_\delta^2 N^2}{2\mu_0 S R^2} = \frac{U^2 (G_\delta + G_l)^2 N^2}{2R^2 \mu_0 S \sigma^2} \tag{8}$$

Further, when $\delta/r_1 \le 0.2$, it can be regarded as the parallel magnetic field between the magnetic plate and magnetic pole [16]. Therefore, the total permeance can be expressed as Eq. (9):

$$G = G_\delta + G_l = \frac{\mu_r \mu_0 S}{l} + \frac{\mu_0 S_g}{\delta} \tag{9}$$

Especially, the S_g can be deduced as Eq. (12) connecting with Eq. (10) and Eq. (11).

$$L = \frac{N^2}{R_m} \tag{10}$$

$$R_m = \frac{l}{\mu_r \mu_0 S} + \frac{\delta}{\mu_0 S_g} \tag{11}$$

$$S_g = 1/\left(\frac{\mu_0 N^2}{L\delta} - \frac{l}{\mu_r \delta S}\right) \tag{12}$$

where S_g and L are the equivalent permeance area of the air gap and inductance individually, μ_r and l are relative

Table 4 Parameters in the simulation process

Process variable	Value	Process variable	Value
Thickness of blank/mm	0.77 (SPCC)	Element type of tool	Rigid shell
Adaptive meshing	Yes	Static friction coefficient between blank and tool	0.1
Contact type between blank and tool	Nonlinear penalty	Dynamic friction coefficient between blank and tool	0.08
Size of air gap/mm	0.3	Area of the cross section of winding/mm^2	6900
Magnitude of current/A	0.6	Element type of distant air	INFIN47

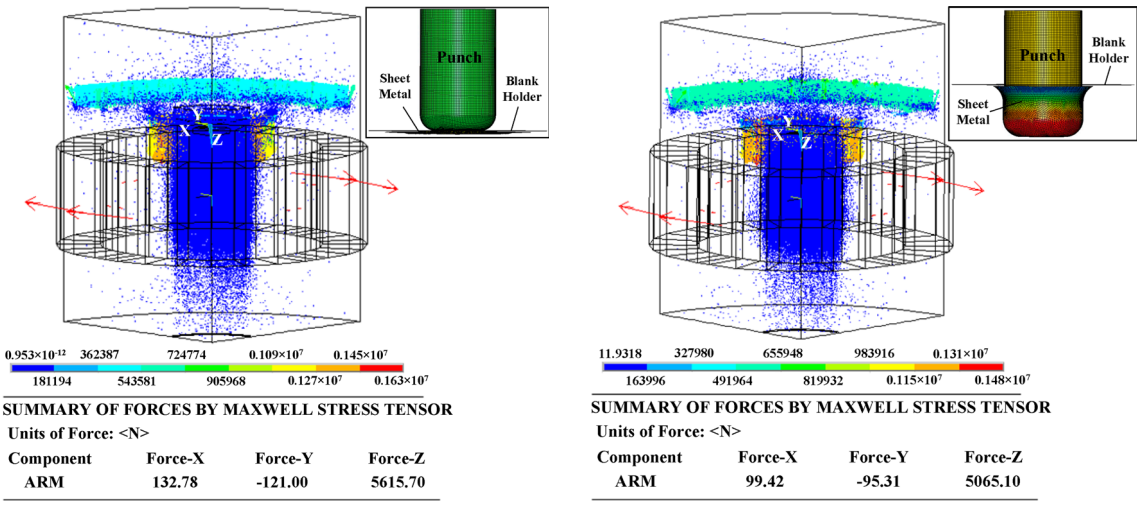

(a) The initial drawing process (b) The terminal drawing process

Fig. 7 Distribution of a magnetic field intensity and corresponding magnitude of EMF. **a** The initial drawing process. **b** The terminal drawing process

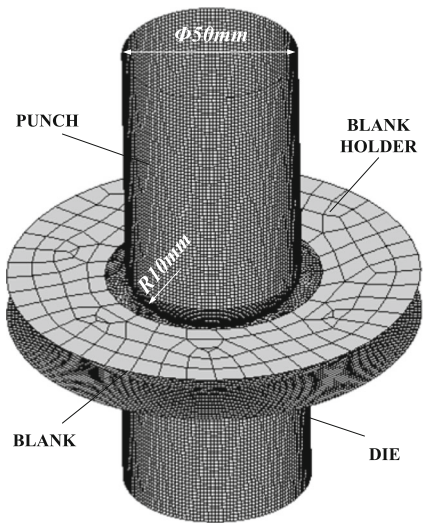

Fig. 8 FE model of drawing tool

permeance of magnetic pole and the average length of the magnetic circuit, and R_m and L are the total magnetic resistance and the created inductance.

Considering that the resistance of inductance can be regarded as zero, the total permeance can be simplified as Eq. (13):

$$G = \frac{\mu_r \mu_0 S}{l} = \frac{\pi \mu_r \mu_0 \left(r_2^2 - r_1^2\right)}{4l} \tag{13}$$

where r_1 and r_2 are the inner and outward margin radius of the magnetic pole.

With substituting the deduced permeance of (3), (4), (13), and $\sigma = 1$ into (8), the EMF equation can be inferred as Eq. (14):

$$F_{\text{mag}} = \frac{\pi U^2 \mu_r^2 \mu_0 \mathrm{N}^2 \left(r_2^2 - r_1^2\right)}{8R^2 l^2} = \frac{U^2 N^2 \mu_r^2 \mu_0 S}{2R^2 l^2} \tag{14}$$

Since the resistance of coils is relative to metal resistivity ρ, length of coils L_{coil} and the area of winding cross-section A_{coil}.

Table 5 Arrangement of simulation testings

Testing number	Magnitude of EMF/N	Testing number	Magnitude of EMF/N
1 (Φ90 mm)	1423	5 (Φ85 mm)	1423
2 (Φ90 mm)	2945	6 (Φ85 mm)	2945
3 (Φ90 mm)	6283	7 (Φ85 mm)	6283
4 (Φ90 mm)	9289	8 (Φ85 mm)	9289

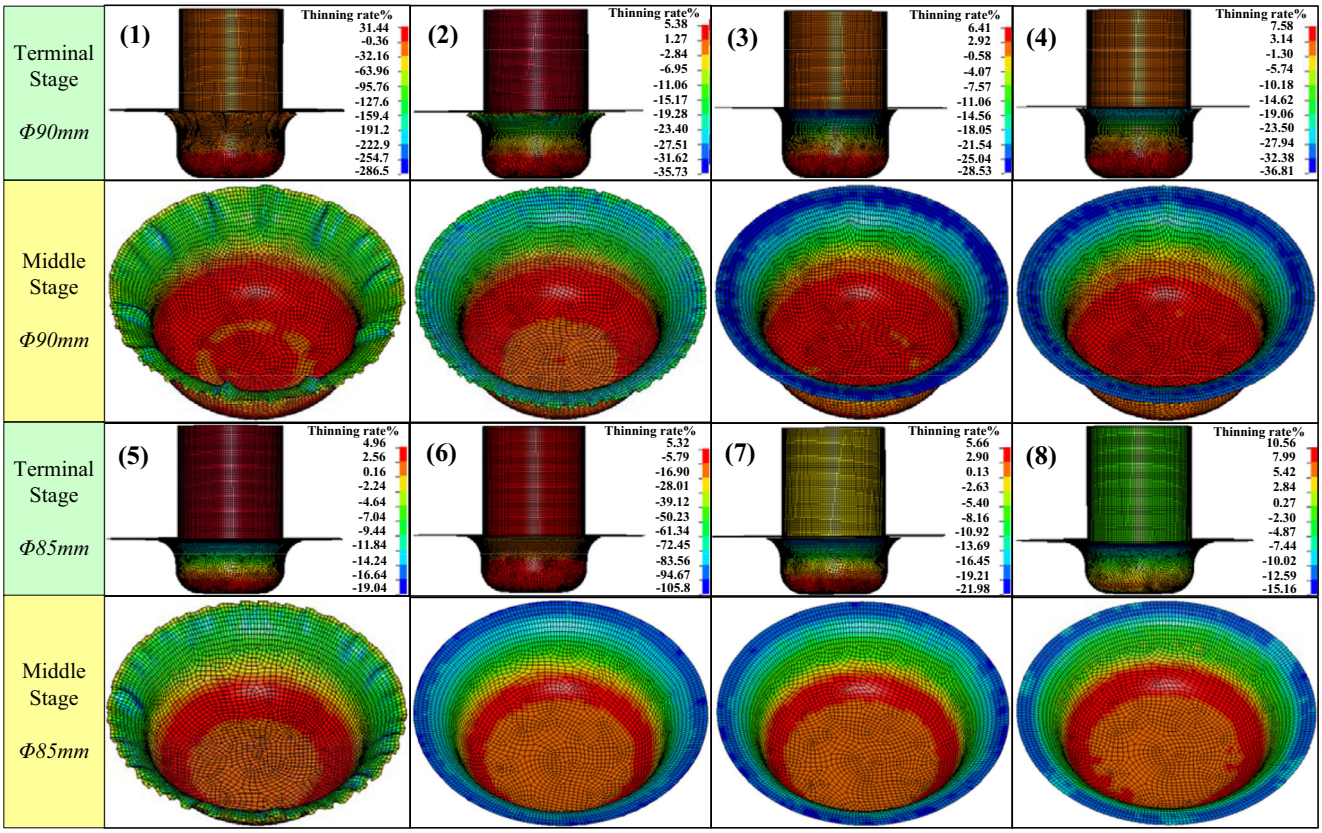

Fig. 9 Drawing results of simulation testings

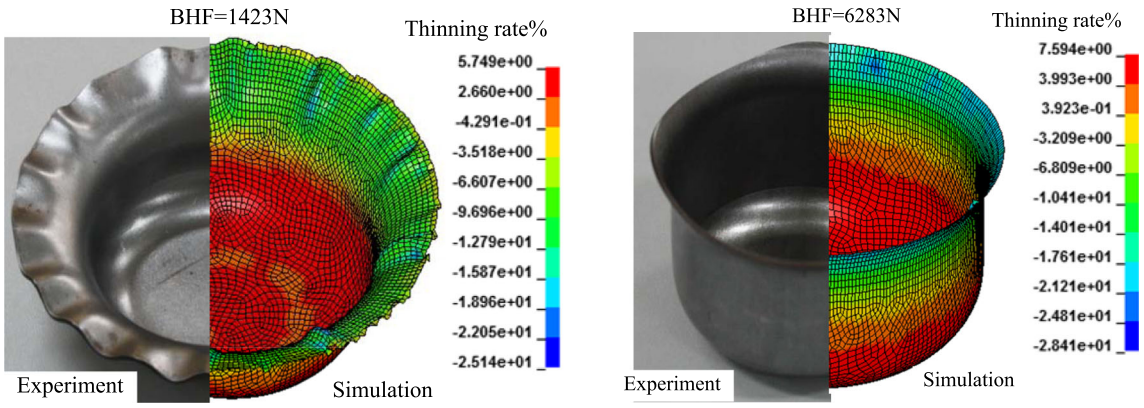

(a) Drawing results under the BHF 1423N (b) Drawing results under the BHF 6283N

Fig. 10 The comparative results between experiment and numerical simulation. **a** Drawing results under the BHF 1423 N. **b** Drawing results under the BHF 6283 N

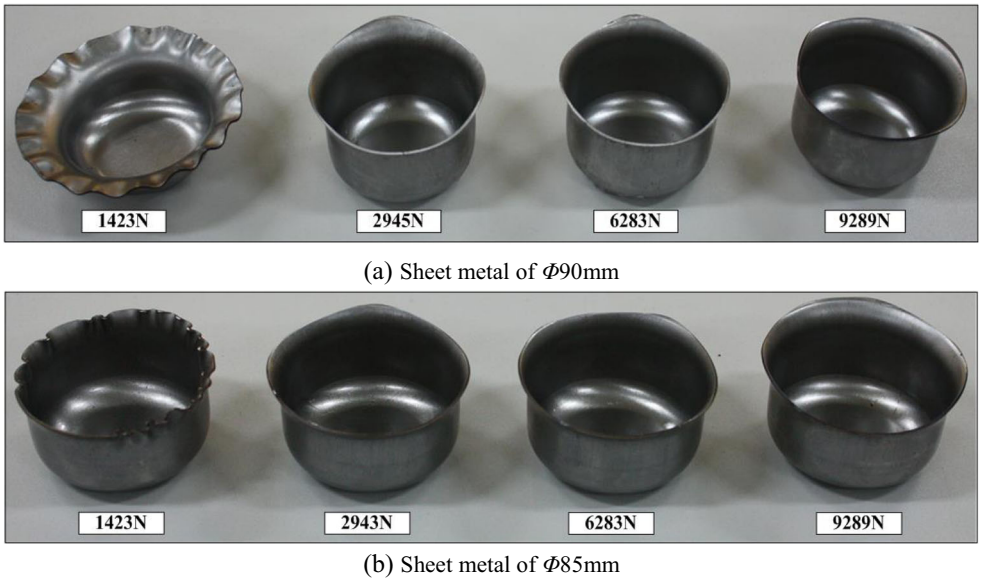

(a) Sheet metal of Φ90mm

(b) Sheet metal of Φ85mm

Fig. 11 Experiment results obtained by EBHS. **a** Sheet metal of Φ90 mm. **b** Sheet metal of Φ85 mm

If not considering the influence of temperature, the relationship expression can be given as Eq. (15):

$$R = \rho \frac{L_{\text{coil}}}{A_{\text{coil}}} \tag{15}$$

Substituting the resistance of coils (15) into (14), concrete expression of EMF can be expressed as Eq. (16):

$$F_{\text{mag}} = \frac{U^2 N^2 \mu_r^2 \mu_0 S A_{\text{coil}}^2}{2l^2 \rho^2 L_{\text{coil}}^2} \tag{16}$$

For clearly expressing the theoretical relationship between EMF and input voltage, concrete parameters of the EBHD are given in Table 3, and the corresponding relationship curve obtained by Eq. (16) has been given in Fig. 6. Additionally, experimental measurement data points have been also displayed in this figure. From Fig. 6, it can be discovered that the theoretical value agrees well with the experimental testing value. Therefore, the feasibility of the deduced EMF formula can be validated.

4 Simulation and experimental validation of EBHS

In order to further explore the feasibility of the designed EBHS, numerical simulation and experimental validation of the cylindrical part deep drawing have been carried out in this study.

To find the distribution of the magnetic field intensity of the initial and the terminal stages of sheet metal drawing process,

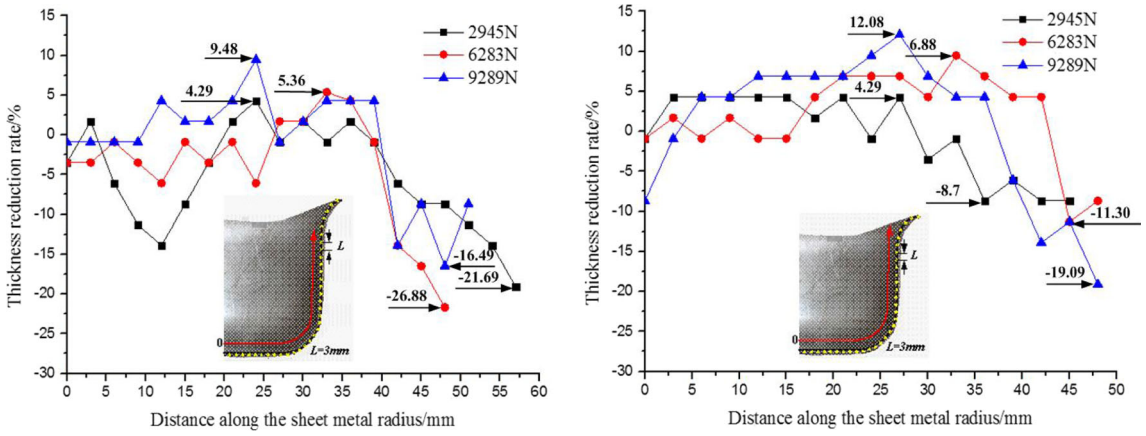

(a) Sheet metal of Φ90mm

(b) Sheet metal of Φ85mm

Fig. 12 Distribution of thickness reduction rate. **a** Sheet metal of Φ90 mm. **b** Sheet metal of Φ85mm

corresponding simulations have been conducted by ANSYS/Multiphysics. An established 3D model has been displayed in Fig. 4. Besides, necessary simulation parameters have been given in Table 4. Figure 7 shows the comparison between the initial and terminal stages of the drawing process.

From Fig. 7, it can be calculated that the magnetic field intensity merely decreases by 9.2% during the whole drawing process. Similarly, the magnitude of EMF decreases by 9.8% from 5616 to 5065 N due to the movement of the punch. Therefore, the influence on the distribution of the magnetic field caused by the movement of drawing tool can be basically neglected in the dynamic simulation of the sheet metal drawing process.

To further validate the effectiveness of EBHS in drawing sheet metal workpiece, numerical simulation of a cylindrical part with applying different BHF has been also conducted by ANSYS/LS-DYNA. Based on the discussion of electromagnetic simulation, simulation parameters of cylindrical part drawing process can be set as a conventional drawing in simulation software. Relative drawing parameters have been listed in Table 4. In addition, established 3D drawing model for the cylindrical part is shown in Fig. 8.

An excellent design for the cylindrical part drawing device is reflected in the formed part without the deficiencies as wrinkling and fracture. According to the literature [30], the thickness distribution of parts will reflect the forming quality of the sheet metal. Therefore, the maximum thickness reduction ratio is also served as one of the evaluation standards of drawing quality in the study. Especially, the maximum thickness reduction of the cup wall should be controlled at a low level to avoid the occurrence of forming defects. Based on the consideration, a group of simulation testings of cylindrical part drawing are implemented, and corresponding magnitudes of BHF are given in Table 5. Eventually, the simulation results of designed testings have been shown in Fig. 9.

From Fig. 9, it can be learned that wrinkling will occur in applying insufficient BHF, such as testing (1), testing (2), and testing (5). When the magnitude of BHF is rationally enhanced, wrinkling of the sheet metal will be effectively eliminated as is shown in testing (3), testing (6), and testing (7). Furthermore, the maximum thinning rate in the three testings is all less than 6.5%, which is at a reasonable level. Whereas, it can be also learned from the results of testing (4) and testing (8) that the thickness reduction rate will exceed the normal amplitude if applying overlarge amplitude of BHF. As a result, it can be preliminarily interpreted that cylindrical part without drawing deficiencies can be obtained through applying reasonable BHF with the usage of EBHS.

To further explore the validation of EBHS, experiments of cylindrical part drawing process have been conducted. Experimental magnitudes of BHF are derived from Table 5, and the other experimental parameters kept in coincidence with that in numerical simulation. For making a comparison with the sheet metal drawing results of numerical simulation and experiment, drawing results of testing (1) and testing (4) realized by the two methods have been shown in Fig. 10. From the results, it can be clearly observed that the simulation results agree well with the experimental results. It is worthy to mention that no deficiency as wrinkling and fracture exists in the drawn cylindrical part with the usage of the BHF 6283 N. Additionally, the thinning rate of cylindrical part is controlled under 7.60%, which is in a reasonable level.

Other than the comparative experiments, other experiments referred to Table 4 have also been carried out. Obtained cylindrical part drawing results are given in Fig. 11. Based on the experiment results, it can be seen that all drawing results of the cylindrical parts have the coincidence with the simulation ones. For further exploring the variation regulation of thickness reduction rate of the cup wall with applying this novel technology, the thickness of the cup wall in testing (2–4) and testing (6–8) has been measured, and corresponding curves of thinning rate along sheet metal radius are depicted in Fig. 12. From Fig. 12, It can be discovered that all the maximum thinning rate and the maximum thickening rate are close to the simulation results and the magnitude of the maximum thickness reduction are all less than 12.10%, which can effectively prove that the EBHS is effective in drawing cylindrical part with high quality.

5 Conclusions

A prototype of the novel EBHS for a conventional drawing process is designed. With the validations by numerical simulations and experiments, corresponding conclusions, and the application prospect of EBHS can be inferred as follows.

(1) Single-coil winding type is beneficial for enhancing EMF.
(2) The magnitude of EMF has a close relationship with the value of input voltage. Especially, the deduced EMF formula that can effectively reflect the relationship between EMF and input voltage.
(3) The movement of drawing tool has poor effectiveness on the created magnetic field of EBHS.
(4) Designed EBHS can effectively improve the forming quality of sheet metal.
(5) Considering that the EBHD is not integrated with the sheet metal drawing system, the novel blank holding system can be also utilized in other stamping system in the future work, such as blanking, bending, and bulging of sheet metal. Besides, workpieces with complicated shapes will be also obtained through alternating the shapes of drawing tools with the usage of EBHD in further research.

References

1. Zhou BJ, Xu YC (2018) The effect of upper sheet on wrinkling and thickness distribution of formed sheet part using double-layer sheet hydroforming. Int J Adv Manuf Technol 99:1175–1182. https://doi.org/10.1007/s00170-018-2432-9
2. Zhao SD, Zhang ZY, Zhang Y, Yuan JH (2007) The study on forming principle in the process of hydro-mechanical reverse deep drawing with axial pushing force for cylindrical cups. J Mater Process Technol 187-188:300–303. https://doi.org/10.1016/j.jmatprotec.2006.11.198
3. Lai ZP, Cao QL, Han XT, Xiong Q, Deng FX, Zhang X, Chen Q, Li L (2016) Design, implementation, and testing of a pulsed electromagnetic blank holder system. IEEE Trans Appl Supercond 26(4): 1–5. https://doi.org/10.1109/TASC.2016.2526028
4. Lai ZP, Cao QL, Zhang B, Han XT, Zhou ZY, Xiong Q, Zhang X, Chen Q, Li L (2015) Radial Lorentz force augmented deep drawing for large drawing ratio using a novel dual-coil electromagnetic forming system. J Mater Process Technol 222:13–20. https://doi.org/10.1016/j.jmatprotec.2015.02.029
5. Lai ZP, Cao QL, Han XT, Huang YJ, Deng FX, Chen Q, Li L (2017) Investigation on plastic deformation behavior of sheet workpiece during radial Lorentz force augmented deep drawing process. J Mater Process Technol 245:193–206. https://doi.org/10.1016/j.jmatprotec.2017.02.010
6. Lai ZP, Cao QL, Han XT, Zhou ZY, Xiong Q, Zhang X, Chen Q, Li L (2014) Radial-axial force controlled electromagnetic sheet deep drawing: electromagnetic analysis. 11th International Conference on Technology of Plasticity (ICTP 2014), October 2014, Procedia Engineering 81:2505–2511. https://doi.org/10.1016/j.proeng.2014.10.358
7. Deng FX, Cao QL, Han XT, Li L (2018) Electromagnetic pulse spot welding of aluminum to stainless steel sheets with a field shaper. Int J Adv Manuf Technol 95:2681–2690. https://doi.org/10.1007/s00170-018-2208-2
8. Cao QL, Han XT, Lai ZP, Xiong Q, Zhang X, Chen Q, Xiao HX, Li L (2015) Analysis and reduction of coil temperature rise in electromagnetic forming. J Mater Process Technol 225:185–194. https://doi.org/10.1016/j.jmatprotec.2015.02.006
9. Huang YJ, Han XT, Cao QL, Lai ZP, Cai H, Liu N, Li XX, Chen M, Li L (2017) Design and analysis of a pulsed electromagnetic blankholder system for electromagnetic forming. International Conference on the Technology of Plasticity (ICTP 2017), September 2017, Procedia Engineering 207:347–352. https://doi.org/10.1016/j.proeng.2017.10.786
10. Seo YR (2008) Electromagnetic blank restrainer in sheet metal forming processes. Int J Mech Sci 50:743–751. https://doi.org/10.1016/j.ijmecsci.2007.11.008
11. Su HL, Huang L, Li JJ, Li GD, Huang P (2017) Investigation on the forming process and the shape control in electromagnetic flanging of aluminum alloy. International Conference on the Technology of Plasticity (ICTP 2017), September 2017, Procedia Engineering 207:335–366. https://doi.org/10.1016/j.proeng.2017.10.784
12. Fan S, Mo JH, Fang JX, Xie J (2018) Electromagnetic pulse-assisted incremental drawing forming of aluminum alloy cylindrical part and its control strategy. Int J Adv Manuf Technol 95:2681–2690. https://doi.org/10.1007/s00170-017-1245-6
13. Fang JX, Mo JH, Li JJ, Cui XH, Fan S (2014) Electromagnetic pulse assisted progressive deep drawing. 11th International Conference on Technology of Plasticity (ICTP 2014), October 2014, Procedia Engineering 81:801–807. https://doi.org/10.1016/j.proeng.2014.10.079
14. Cui XH, Mo JH, Fang JX, Li JJ (2014) Deep drawing of cylindrical cup using incremental electromagnetic assisted stamping with radial magnetic pressure. 11th International Conference on Technology of Plasticity (ICTP 2014), October 2014, Procedia Engineering 81: 813–818. https://doi.org/10.1016/j.proeng.2014.10.081
15. Fang JX, Mo JH, Cui XH, Li JJ, Zhou B (2016) Electromagnetic pulse-assisted incremental drawing of aluminum cylindrical cup. J Mater Process Technol 238:395–408. https://doi.org/10.1016/j.jmatprotec.2016.07.029
16. Cui XH, Li JJ, Mo JH, Fang JX, Zhu YT, Zhong K (2015) Investigation of large sheet deformation process in electromagnetic incremental forming. Mater Des 76:86–96. https://doi.org/10.1016/j.matdes.2015.03.060
17. Cui XH, Mo JH, Li JJ, Xiao XT, Zhou B, Fang JX (2016) Large-scale sheet deformation process by electromagnetic incremental forming combined with stretch forming. J Mater Process Technol 237:139–154. https://doi.org/10.1016/j.jmatprotec.2016.06.004
18. Cui XH, Mo JH, Li JJ, Zhao J, Zhu Y, Huang L, Li ZW, Zhong K (2014) Electromagnetic incremental forming (EMIF): a novel aluminum alloy sheet and tube forming technology. J Mater Process Technol 214:409–427. https://doi.org/10.1016/j.jmatprotec.2013.05.024
19. Cui XH, Yu HL, Wang QS (2018) Reduction of corner radius of cylindrical parts by magnetic force under various loading methods. Int J Adv Manuf Technol 97:2667–2674. https://doi.org/10.1007/s00170-018-2111-x
20. Wang QX, Wu ZF, Wang DQ, Fu XY (2017) Study of measurement method for large imbalance evaluation based on dynamic electromagnetic force. Measurement 104:142–150. https://doi.org/10.1016/j.measurement.2017.03.020
21. Paese E, Geier M, Homrich RP, Rossi R (2015) A coupled electric-magnetic numerical procedure for determining the electromagnetic force from the interaction of thin metal sheets and spiral coils in the electromagnetic forming process. Appl Math Model 39:309–321. https://doi.org/10.1016/j.apm.2014.05.032
22. Okoye CN, Jiang JH, Hu ZD (2006) Application of electromagnetic-assisted stamping (EMAS) technique in incremental sheet metal forming. Int J Mach Tool Manu 46:1248–1252. https://doi.org/10.1016/j.ijmachtools.2006.01.029
23. Akbar S, Awan MS, Aleem MA, Sarwar MN, Farooque M (2015) Effect of field intensity on electromagnetic flat sheet forming. Materials Today: Proceedings 2(5):324–5328. https://doi.org/10.1016/j.matpr.2015.11.044
24. Guo K, Lei XP, Zhan M, Tan JQ (2017) Electromagnetic incremental forming of integral panel under different discharge conditions. J Manuf Process 28:373–382. https://doi.org/10.1016/j.jmapro.2017.01.010
25. Shang JH, Daehn G (2011) Electromagnetically assisted sheet metal stamping. J Mater Process Technol 211:868–874. https://doi.org/10.1016/j.jmatprotec.2010.03.005
26. Arumugam P, ShanmugaSundaram K, KamalaKannan N (2014) Experimental study of electromagnetic sheet metal forming process. 12th Global Congress on Manufacturing and Management (GCMM 2014), Procedia Engineering 97:277–290. https://doi.org/10.1016/j.proeng.2014.12.251
27. Long AL, Wan M, Wang WP, Wu XD, Cui XX, Ma BL (2017) Forming methodology and mechanism of a novel sheet metal forming technology-electromagnetic superposed forming (EMSF). Int J Solids Struct 151:1–16. https://doi.org/10.1016/j.ijsolstr.2017.11.003
28. Li S, Cui XY, Li GY (2018) Modelling and demonstration of electromagnetically assisted stamping system using an interactive mapping method. Int J Mech Sci 144:312–323. https://doi.org/10.1016/j.ijmecsci.2018.06.003

29. Liu DH, Li CF, YU HP (2009) Numerical modeling and deformation analysis for electromagnetically assisted deep drawing of AA5052 sheet. Trans Nonferrous Metals Soc China 19:1294–1302. https://doi.org/10.1016/S1003-6326(08)60441-0

30. Cui XL, Zhan M, Gao PF, Ma F, Guo J, Li R, Li ZX, Zhang HR (2018) Influence of blank thickness fluctuation on flange state and final thickness distribution in the power spinning of thin-walled head. Int J Adv Manuf Technol 99:363–372. https://doi.org/10.1007/s00170-018-2486-8